# Design optimization of highly sensitive LSPR enhanced surface plasmon resonance biosensors with nanoholes

**Bin Wu (吴 斌) and Qingkang Wang (王庆康)**

*National Key Laboratory of Micro/Nano Fabrication Technology, Key Laboratory for Thin Film and Microfabrication Technology of Ministry of Education, Research Institute of Micro/Nano Science and Technology, Shanghai Jiao Tong University, Shanghai 200030*

Received November 23, 2007

For breaking through the sensitivity limitation of conventional surface plasmon resonance (SPR) biosensors, novel highly sensitive SPR biosensors with Au nanoparticles and nanogratings enhancement have been proposed recently. But in practice, these structures have obvious disadvantages. In this study, a nanohole based sensitivity enhancement SPR biosensor is proposed and the influence of different structural parameters on the performance is investigated by using rigorous coupled wave analysis (RCWA). Electromagnetic field distributions around the nanohole are also given out to directly explain the performance difference for various structural parameters. The results indicate that significant sensitivity increase is associated with localized surface plasmons (LSPs) excitation mediated by nanoholes. Except to outcome the weakness of other LSP based biosensors, larger resonance angle shift, reflectance amplitude, and sharper SPR curves' width are obtained simultaneously under optimized structural parameters.

*OCIS codes:* 130.3120, 230.3990, 040.1880.

Surface plasmon resonance (SPR) has been widely used in a variety of sensing applications, since it provides rapid, label-free and array-based real-time sensing capability of detecting biochemical reactions on surface. The attenuated total internal reflection method has been widely used to excite surface plasmons in conventional SPR biosensors, such as Kretschmann configuration[1]. This kind of biosensor is extremely simple in structure and has been commercially available. However, its sensitivity is not high enough for some applications, such as sensing of aerosol or gas-phase release of toxins.

In order to overcome the sensitivity limitation, nanoparticle-based SPR biosensors have drawn tremendous interests, since it has been empirically shown that applying nanoparticles may significantly enhance its sensitivity by $1-2$ orders of magnitude[2−6]. The use of noble metal nanostructures allows strong optical coupling of incident light to resonances, so called localized surface plasmons (LSPs). Various interactions among LSPs, surface plasmon polaritons (SPPs), and binding biomaterial in the presence of nanostructures can lead to different resonance properties with an additional shift of resonance angle, and changes in the reflectance amplitude and resonance width, resulting in enhanced sensitivity of a SPR biosensor.

Recently, it is proved that nanograting structure can also lead to similar enhancement[7,8]. Compared with nanoparticles, nanograting structure shows great advantage for it can be made by conventional micro-electronic fabrication technology with high throughput. But it also has obvious disadvantages. Firstly, when the analytes solution contains huge biomolecules, the biosensor has the risk to lock them in nanogrooves and make mistakes. The antibody analyte binding films are also hard to be placed and cleaned up. Secondly, though the nanograting structure brings huge shift of the resonance angle, it brings wider SPR curves and lower reflective amplitudes too. In practice, the angle location of the resonance peak is difficult to be found in this situation. For avoiding these two weaknesses, we propose a novel structure that employs nanoholes which also can bring sensitivity enhancement. This structure has a flat surface for sensing and has the ability to balance the three factors of sensitivity. The model is studied using well-established rigorous coupled wave analysis (RCWA)[9−14]. We are particularly interested in the impact of geometrical parameters such as nanohole period and its profile and size on the performance in this novel biosensor.

A schematic diagram of a nanohole-based SPR biosensor model is shown in Fig. 1, where nanoholes are represented as a one-dimensional (1D) array sit in thin film of a gold layer, oriented along the $y$-axis. In this paper we only investigate the case of rectangular nanoholes, so the profile of nanoholes is decided by the width and height. In the diagram, $d_{\rm f}$ represents the thickness of the gold film (fixed at 55 nm in this paper), and $d_{\rm h}$, $d_{\rm t}$, and $d_{\rm b}$ represent the nanohole height, the thickness of the top film on the nanoholes and the thickness of the base film (fixed at 25 nm in this paper) under nanoholes, respectively. $\Lambda$ is defined as the period of the nanohole array. The relation between the width of the nanohole $w$ and the period of the nanohole array $\Lambda$ is $f=\frac{w}{\Lambda}$. There, $f$ has

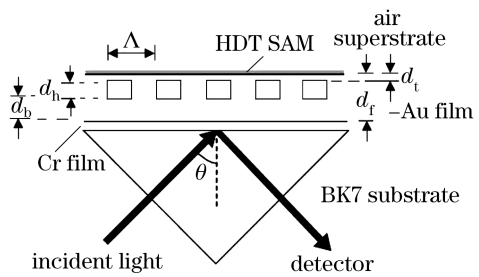


Fig. 1. Schematic of a nanohole-based SPR biosensor.

1671-7694/2008/050323-04 

the meaning of inverse fill factor. An 2-nm thick attachment layer of chromium is placed between the thin gold film and BK7 glass prism for good contact. The antibody analyte binding is modeled with a 1-nm thick self-assembled monolayer (SAM) that is supported by the thin gold film. The complex refractive indices of the BK7 glass prism substrate, layer of chromium, and gold were taken from Ref. [15], determined respectively as 1.5151, $3.48 + 4.36i$, and $0.18 + 3.0i$ at $\lambda = 633$ nm. In our study, we assumed SAM has the refractive index of 1.526. The model in Fig. 1 assumes an illumination with a TM-polarized monochromatic plane wave at a fixed wavelength $\lambda = 633$ nm as the incidence angle $\theta$ is scanned with an angular resolution of 0.01°.

As a quantitative measure of the sensitivity improvement, we introduce a sensitivity enhancement factor (AS-SEF, similar as SEF in Ref. [8]) to represent the impact of nanoholes on the SPR angle shift enhancement in reference to the conventional SPR biosensor without nanostructures as:

$$\mathrm{AS-SEF} = \left|\frac{\Delta\theta_{\mathrm{NHSPR}}}{\Delta\theta_{\mathrm{SPR}}}\right| = \left|\frac{\theta_{\mathrm{NHSPR}}(\mathrm{analyte}) - \theta_{\mathrm{NHSPR}}(\mathrm{noanalyte})}{\theta_{\mathrm{SPR}}(\mathrm{analyte}) - \theta_{\mathrm{SPR}}(\mathrm{noanalyte})}\right|, \quad (1)$$

where $\Delta\theta$ is the difference between the plasmon resonance angles with and without analytes, and the subscripts NHSPR and SPR represent a nanohole-enhanced SPR configuration and a conventional SPR scheme, respectively.

Figure 2 shows the SPR curves of the nanohole SPR biosensor and conventional SPR biosensor. The resonance angle shift of the conventional SPR biosensor is 0.15° and that of the nanohole biosensor is 0.59°. In Fig. 2, the AS-SEF is calculated to be 3.93 and the width of the SPR curves is also broadened at the same time. For SPR curve with larger width and smaller reflectance amplitude, it is more difficult to find the resonance angle, so it is necessary to obtain sharper curves under the condition of larger AS-SEF and amplitude. In the following, the effect of the structural parameters on the performance of the nanohole biosensor is discussed.

The plot of AS-SEF versus period nanoholes and SPR curves for different periods are shown in Fig. 3. The

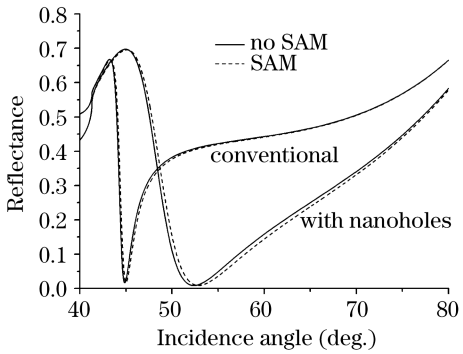


Fig. 2. SPR curves of nanohole biosensor and conventional SPR biosensor. For the conventional biosensor, the structure parameter is $d_{\mathrm{f}} = 55$ nm. For the nanohole biosensor, the structure parameters are $d_{\mathrm{t}} = 5$ nm, $f = 0.2$, and $\Lambda = 40$ nm.

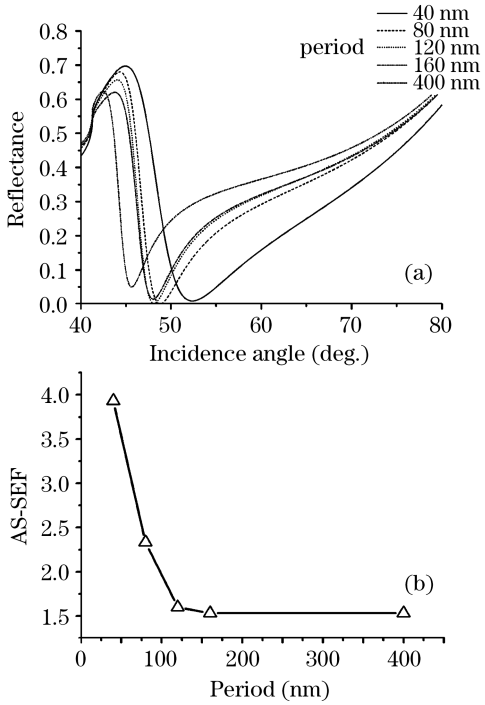


Fig. 3. (a) SPR curves for different periods and (b) plot of AS-SEF versus period. $d_t$ and $f$ of the nanohole biosensor are 5 nm and 0.2, respectively.

calculated results show that the AS-SEF, the width and reflective amplitude of SPR curves decrease as the period enlarges. The highest AS-SEF is 3.93 with the period of 40 nm and the lowest one is 1.53 with the period of 400 nm.

The AS-SEF with the period of 40 nm is the highest, but the SPR curves' width is larger than other situations. On the other hand, although the SPR curve is the narrowest with period of 400 nm, the AS-SEF and reflectance amplitude are not good and the reflectance amplitude is smaller, so a balance of these three factors should be searched. In this paper, although there is a relative wide curves width when the period of the nanoholes is 40 nm, it is still not difficult to find the resonance angle. So the period of 40 nm is selected for the investigations of the largest AS-SEF.

Sensitivity of the nanoholes biosensors with filling factor varying is then investigated. The calculated curves are given out in Fig. 4, which show that the change of AS-SEF, curves' width, and reflectance amplitude with filling factors. The inverse filling factors of 0.1 and 0.8 show the lowest AS-SEF. In the case of 0.1, the nanohole is very confined. The whole gold film is close to the conventional flat film. Relatively, in the case of 0.8, the volume of nanohole is very large. The whole gold film is close to two parallel conventional flat films with an air interval. So in these two cases, the AS-SEF is close to conventional SPR biosensor. The highest AS-SEF is 4.07 with a inverse filling factor of 0.6. Then, the AS-SEF is 3.93 with a inverse filling factor of 0.2. Although the AS-SEF at $f = 0.6$ is larger than that at $f = 0.2$, the width and amplitude of SPR curves at $f = 0.6$ is worse than that at $f = 0.2$. So in designing of SPR biosensor, $f = 0.2$ is preferred with other parameters fixed.

We also investigate the influence of this thin gold

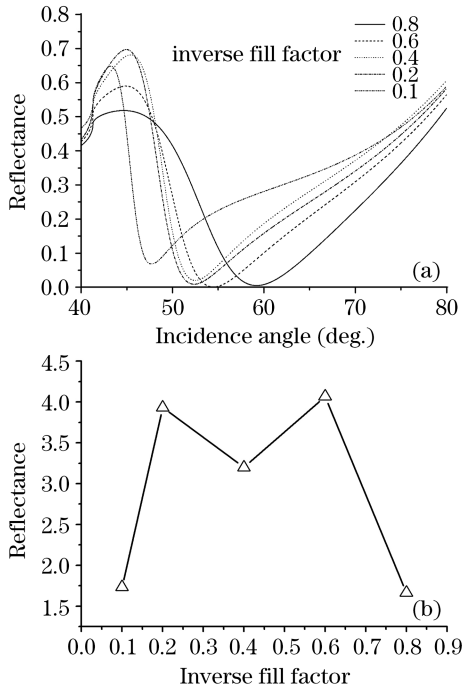


Fig. 4. (a) SPR curves for different inverse fill factors and (b) plot of AS-SEF versus inverse fill factor. $d_t$ and $\Lambda$ of the nanohole biosensor are 5 nm and 40 nm, respectively.

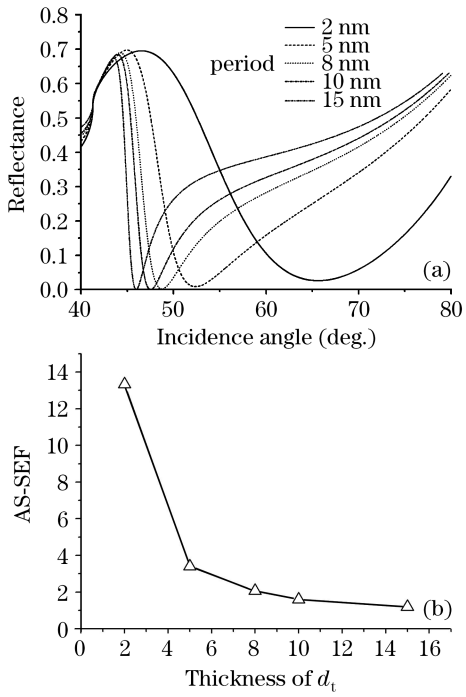


Fig. 5. (a) SPR curves for different thicknesses of $d_t$ and (b) plot of AS-SEF versus inverse fill factor. $\Lambda$ and $f$ of the nanohole biosensor are 40 nm and 0.2, respectively.

film on the top of 1D nanoholes on the sensitivity of the biosensor. The calculated results are given out in Fig. 5. The curves' width and AS-SEF enhance, but the reflectance amplitude decrease as $d_t$ increasing. So this film has the function of adjusting the profile of SPR curves. Although the AS-SEF with $d_t = 2$ nm is the largest, the width of the SPR curves is too large to exactly find the resonance angle. Considering both the curves' width and AS-SEF enhance, $d_t = 5$ nm is the best choice.

For visualizing the fields, the spatial distribution of the magnetic field amplitudes in one period at resonance has been calculated based on RCWA for a conventional thin film based structure and nanhole structures in Fig. 6. For Figs. 6(b)—(e), the one period model sets two half nanohole on the side and gold part in the middle. It is assumed that no SAM exists.

In Fig. 6(a), it is clear that the SPR resonance energy is concentrated on the top side of the flat gold film. However, in Fig. 6(b), the strongest magnetic field is in the nanohole (white in the picture). It is clearly conveyed that the structures show localized field distribution and completely delocalized for the thin film base. So, these results, combined with the data presented in Fig. 2, strongly suggest that the field localization introduced by nanoholes is intimately connected to the localized surface plasmon resonance (LSPR) enhancement and the sensitivity improvement. Figure 6(c) shows that magnetic intensity in the nanohole decreases with period increasing, compared with Fig. 6(b). We only provide the distribution at the period of 400 nm, but the distribution at other periods, not shown here, also confirms this trend. The reason for this trend is that stronger LSPR enhancement happens at a smaller nanohole period in this range, as shown in Fig. 3(b). The magnetic field distribution situation in Fig. 6(d) shows that too large inverse fill factor will decrease the LSPR of nanoholes. With inverse fill factor of 0.8, the whole gold film is close to two parallel flat films with an interval between them. The light

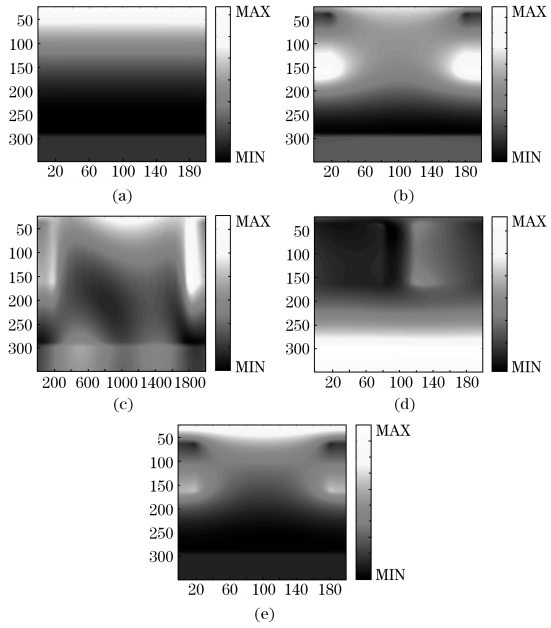


Fig. 6. Spatial distribution of the magnetic field amplitude at resonance, calculated by RCWA . We only provide the magnetic field distribution in one period (0.2 nm for one unit in the figure). (a) Conventional film without nanoholes; (b) nanohole-based structure with $d_t = 5$ nm, $f = 0.2$, and $\Lambda = 40$ nm; (c) nanohole-based structure with $d_t = 5$ nm, $f = 0.2$, and $\Lambda = 400$ nm; (d) nanohole-based structure with $d_t = 5$ nm, $f = 0.8$, and $\Lambda = 40$ nm; (e) nanohole-based structure with $d_t = 15$ nm, $f = 0.2$, and $\Lambda = 40$ nm.

energy cannot bring to the top film without enough gold joining. So the energy is damping in the upside, and it can be found that the stronger LSPR enhancement needs appropriate inverse fill factor, which is not too large or too small. For example, 0.2 and 0.6 are feat, as shown in Fig. 4(b). In Fig. 6(e), $d_{\rm t}$ is up to 15 nm. It is obvious that the magnetic field amplitudes in the nanohole decrease with $d_{\rm t}$ increasing, comparing with Fig. 6(b). This means the LSPR enhancement also weakens. In the same time, the bulk SPR effect increases, because some of the energy transfers to the upside of the film. The distribution at other $d_{\rm t}$, not shown here, also confirms this trend, as shown in Fig. 5(b).

This work proposed a novel nanohole-based LSPR biosensor and presents a comprehensive optimization analysis for the dependence of performance on structural parameters in it using RCWA. This structure outcomes the disadvantages of the nanoparticle and nanograting structures and also shows strong sensitivity improvement in comparison with a conventional SPR structure. More specifically, resonant angle shift, width, and amplitude of the SPR curves are considered simultaneously to optimize the sensitivity enhancement by changing the structural parameters. According to our simulated results, the nanohole biosensor with $d_{\rm t} = 5$ nm, $d_{\rm h} = 25$ nm, $d_{\rm b} = 25$ nm, $f = 0.2$, and $\Lambda = 40$ nm performs best when the three factor are considered. What is more, the electric field distribution around the nanoholes is given to directly explain the performance difference for the conventional structure and nanohole structure. But the problem is that in order to excite LSPs through nanoholes, extremely fine nanoholes should be fabricated with precision to optimally tune both the period and the separation, which are more difficult than nanogratings.

This work was supported by the Nanotechnology Programs of Science and Technology Commission of Shanghai Municipality under Grant No. 0652nm004. B. Wu's e-mail address is binwu@sjtu.edu.cn.

## References

1. E. Kretschmann and H. Raether, Z. Naturforsch. **23A,** 2135 (1968).
2. L. He, M. D. Musick, S. R. Nicewarner, F. G. Salinas, S. J. Benkovic, M. J. Natan, and C. D. Keating, J. Am. Chem. Soc. **122,** 9071 (2000).
3. M. D. Malinsky, K. L. Kelly, G. C. Schatz, and R. P. V. Duyne, J. Am. Chem. Soc. **123,** 1471 (2001).
4. A. J. Haes and R. P. V. Duyne, J. Am. Chem. Soc. **124,** 10596 (2002).
5. A. D. McFarland and R. P. V. Duyne, Nano Lett. **3,** 1057 (2003).
6. S.-J. Chen, F. C. Chien, G. Y. Lin, and K. C. Lee, Opt. Lett. **29,** 1390 (2004).
7. K. M. Byun, S. J. Kim, and D. Kim, Appl. Opt. **45,** 3382 (2006).
8. D. Kim, J. Opt. Soc. Am. A **23,** 2307 (2006).
9. Y. Kanamori, K. Hane, H. Sai, and H. Yugami, Appl. Phys. Lett. **78,** 142 (2001).
10. S. Park, G. Lee, S. H. Song, C. H. Oh, and P. S. Kim, Opt. Lett. **28,** 1870 (2003).
11. E. Moreno, D. Erni, C. Hafner, and R. Vahldieck, J. Am. Opt. Soc. A **19,** 101 (2002).
12. L. Zhang and C. Li, Chinese J. Lasers (in Chinese) **33,** 467 (2006).
13. L. Zhang, C. Li, and F. Zhang, Chinese J. Lasers (in Chinese) **33,** 805 (2006).
14. Z. Hu, A. Yan, D. Liu, X. Wang, and L. Liu, Acta Opt. Sin. (in Chinese) **26,** 1127 (2006).
15. E. D. Palik, *Handbook of Optical Constants of Solids* (Academic Press, New York, 1985).